Author Manuscript

Author Manuscript

Author Manuscript

Author Manuscript

HHS Public Access

Author manuscript

Phys Med Biol. Author manuscript; available in PMC 2018 September 15.

Published in final edited form as:

Phys Med Biol. ; 62(19): 7765–7783. doi:10.1088/1361-6560/aa8803.

Improving Image Quality for Digital Breast Tomosynthesis: Automated Detection and Diffusion-based Method for Metal Artifact Reduction

Yao Lu[*], **Heang-Ping Chan**, **Jun Wei**, **Lubomir M. Hadjiiski**, and **Ravi K. Samala**

Department of Radiology, University of Michigan, Ann Arbor, MI, USA

Abstract

In digital breast tomosynthesis (DBT), the high-attenuation metallic clips marking a previous biopsy site in the breast cause errors in the estimation of attenuation along the ray paths intersecting the markers during reconstruction, which result in interplane and inplane artifacts obscuring the visibility of subtle lesions. We proposed a new metal artifact reduction (MAR) method to improve image quality. Our method uses automatic detection and segmentation to generate a marker location map for each projection (PV). A voting technique based on the correlation among different PVs is designed to reduce false positives (FPs) and to label the pixels on the PVs and the voxels in the imaged volume that represent the location and shape of the markers. An iterative diffusion method replaces the labeled pixels on the PVs with estimated tissue intensity from the neighboring regions while preserving the original pixel values in the neighboring regions. The inpainted PVs are then used for DBT reconstruction. The markers are repainted on the reconstructed DBT slices for radiologists' information. The MAR method is independent of reconstruction techniques or acquisition geometry. For the training set, the method achieved 100% success rate with one FP in 19 views. For the test set, the success rate by view was 97.2% for core biopsy microclips and 66.7% for clusters of large post-lumpectomy markers with a total of 10 FPs in 58 views. All FPs were large dense benign calcifications that also generated artifacts if they were not corrected by MAR. For the views with successful detection, the metal artifacts were reduced to a level that was not visually apparent in the reconstructed slices. The visibility of breast lesions obscured by the reconstruction artifacts from the metallic markers was restored.

Keywords

digital beast tomosynthesis; metal artifact reduction; diffusion method; automated detection; image quality

Correspondence: Heang-Ping Chan, Ph.D., Department of Radiology, University of Michigan, 1500 E. Medical Center Drive, C477 Med-Inn Bldg, Ann Arbor, MI 48109-5842, Telephone: (734) 936-4357, chanhp@umich.edu.

[*]Current address: School of Data and Computer Science, Sun Yat-sen University, Guangzhou, China

Author Manuscript Author Manuscript Author Manuscript Author Manuscript

I. INTRODUCTION

Digital breast tomosynthesis (DBT) is a new imaging modality that utilizes limited-angle computed tomography technology to provide quasi-three-dimensional (3D) structural information of the breast (Niklason *et al* 1997, Kopans 2001). DBT can reduce tissue overlap and improve the visualization of normal tissue and suspicious masses. A number of studies showed that DBT as an adjunct to mammography increased the sensitivity for detecting breast cancer and reduced recall rate in comparison to mammography alone (Ciatto *et al* 2013, Rose *et al* 2013, Skaane *et al* 2013a, Skaane *et al* 2013b, Friedewald *et al* 2014, Durand *et al* 2015, Bernardi *et al* 2016, Conant *et al* 2016, Gilbert *et al* 2016, Sharpe *et al* 2016).

Current DBT systems utilize limited-angle cone-beam geometry. A DBT system acquires a small number of low-dose x-ray projections (PVs) of the breast at different projection angles over a limited angular range. DBT systems that have been built to-date acquire 9–25 individual PVs with fixed or variable angular increments of 1° – 5° within an angular range of 16° – 60° (Sechopoulos 2013, Chan *et al* 2014, Goodsitt *et al* 2014). Because of the incomplete acquisition of projection data from a limited scan angular range, tomosynthesis reconstruction suffers from severe interplane and inplane artifacts around high-contrast objects such as metallic markers. Metal artifact arises from the high-attenuation metallic markers embedded in the breast from a previous biopsy. X-rays intersecting a metallic object are highly attenuated and few photons can reach the detector. During reconstruction, the affected pixels in the PVs cause errors in the estimation of attenuation along the ray paths intersecting the metallic object. Because of the severe undersampling of projections in DBT system, the voxel value errors in the artifact region cannot be compensated for from other PVs. This causes stronger metal artifacts for DBT than those for CT reconstruction. The metal artifacts affect the visibility and detectability of lesions in the reconstructed DBT images.

Metal artifact reduction (MAR) has been widely studied for general computed tomography (CT) applications. Abdolli *et al.* (Abdoli *et al* 2012) reviewed the MAR strategies for CT/PET imaging. Gjesteby *et al.* (Gjesteby *et al* 2016) more recently reviewed the current status of MAR in CT. The majority of these MAR algorithms were designed to correct the sinogram from CT imaging and were applicable to either non-iterative or iterative reconstruction methods. The affected region is either segmented in the sinogram domain (Lewitt 1979, Glover and Pelc 1981, Veldkamp *et al* 2010) or detected in the image domain and then forward projected to the sinogram domain (Kalender *et al* 1987, Zhao *et al* 2000, Mahnken *et al* 2003). For non-iterative reconstruction methods such as filtered backprojection (FBP), the MAR algorithms directly compensate for the reduced intensities at the metal-affected detector bins in the sinogram. One approach is to use interpolation methods such as linear interpolation (Lewitt 1979), smooth interpolation (Veldkamp *et al* 2010), cubic interpolation (Bazalova *et al* 2007), spline interpolation (Abdoli *et al* 2010) and wavelet-based interpolation (Zhao *et al* 2000). Another approach is to exploit the anatomical information or sparsity property of the imaged data to compensate for the missed region by the metallic implant (Bal and Spies 2006, Mehranian *et al* 2011). For iterative reconstruction methods such as the simultaneous algebraic reconstruction technique (SART) or the

Author Manuscript Author Manuscript Author Manuscript Author Manuscript

maximum likelihood (ML) method, the first few iterations may give a rough estimate of the voxel value distribution of the imaged volume. The interpolation-based method, model-based method or sparsity-based method can be used to estimate the compensation required for the artifact region. The compensated volume is then forward projected to the sinogram region to replace the affected sinogram bins (De Man *et al* 2000, Nuyts and Stroobants 2005, Zhang *et al* 2011, Verburg and Seco 2012). The non-iterative reconstruction methods can also use a similar approach by reconstructing multiple times (Abdoli *et al* 2010, Boas and Fleischmann 2011).

DBT system has few PVs from only a small angular range, but each covers a relatively large field of view compared to CT. The metallic objects in a breast are mostly biopsy clips of various sizes and shapes. Geometric unsharpness due to x-ray focal spot and reconstruction may cause blurred edges around the object in the reconstructed slices, which brings uncertainties at the boundary of the artifact region in the reconstructed breast volume. The ideas of the MAR methods for general CT applications may be adapted to DBT, taking into consideration the characteristics of DBT imaging. Several studies have proposed methods for removing metal artifacts for digital tomosynthesis (Chakraborty *et al* 1984, Badea *et al* 1998, Claus and Eberhard 2002, Wu *et al* 2006, Ge *et al* 2007a, Levakhina *et al* 2013). An interpolation method was applied along the direction of the blur or in the wavelet domain of the reconstructed image volume (Chakraborty *et al* 1984, Badea *et al* 1998). Ge et al. applied a deblurring technique to the artifact region based on 3D geometric information in the reconstruction space (Ge *et al* 2007a). However, the interpolation methods or deblurring technique may introduce new artifacts. Other investigators (Claus and Eberhard 2002, Wu *et al* 2006, Levakhina *et al* 2013) identified the PVs that contributed to the artifacts for the reconstructed voxels in the artifact region and assigned different weights to different PVs during the reconstruction, with less or zero weight to the identified affected PVs. With the weighting method, if the affected rays in some PVs are excluded (zero weight) from the reconstruction, the voxels inside the artifact region will obtain unequal number of PV updating compared to the voxels outside the artifact region, potentially causing discontinuous changes in the gray levels inside and outside the artifact region in the reconstructed volume. If non-zero weights are assigned to the affected PVs, residual high-contrast artifacts may be left in the DBT images because of the high attenuation of metallic clips compared to that of the surrounding soft tissue.

In this study, we developed a new diffusion-based PV inpainting method for MAR in DBT (Lu *et al* 2013b). A fully automated feature-based detection and segmentation method was used to generate a metallic clip location map for each PV. The correlation among different PVs was analyzed to reduce false positive (FP) detections. An iterative diffusion method was designed to replace the labeled clip pixels with estimated tissue intensity from the neighboring regions in each PV. The inpainted PVs were then used for DBT reconstruction. If the metal markers are detected and inpainted correctly in all PVs, the reconstructed volume will be free of metal artifacts. The proposed MAR method is applicable to DBT acquired with any imaging system geometry (e.g., tomographic scan angle and angular increments) and reconstruction techniques.

Author Manuscript Author Manuscript Author Manuscript Author Manuscript

Recently, Wicklein *et al.* presented a MAR method for DBT (Wicklein *et al* 2017). The basic approach is similar to ours, namely, they also removed the high-contrast objects on the projection images before reconstruction. The specific techniques used in each step were different, however, based on the brief description in the conference paper. In particular, they did not use a diffusion-based inpainting method to refill the missing tissue intensity in the regions where a high-contrast object was removed, and their method was specifically designed for FBP reconstruction such that they had to filter the tissue-only projections and original projections separately to avoid undershooting artifacts at metal borders. The details of our methods are described below.

II. MATERIALS AND METHODS

A. Breast Tomosynthesis System

In this study, we used a GE prototype GEN2 DBT system in our research laboratory for image acquisition. Figure 1 shows the imaging geometry of this DBT system. The x-ray source rotates in a plane parallel to the chest wall and perpendicular to the detector plane. The distance from the x-ray focal spot to the fulcrum of rotation is 64 cm. The system has a flat panel detector with a CsI phosphor/a:Si active matrix of 1920 × 2304 pixels and a pixel pitch of 0.1 mm × 0.1 mm. The digital detector is stationary during image acquisition. The system uses a step-and-shoot design and can acquire DBT scan with variable combinations of number of projections and angular increments (Chan *et al* 2014, Goodsitt *et al* 2014). The DBT system uses an Rh-anode/Rh-filter x-ray source for all breasts.

We implemented SART for DBT reconstruction. The voxel dimensions of the imaged volume in both the X and Y directions were chosen to be 0.1 mm, the same as the pixel pitch of the detector. The slice spacing in the Z direction was chosen to be 1 mm. The details of our reconstruction method have been described elsewhere (Zhang *et al* 2006, Lu *et al* 2010, Lu *et al* 2015).

B. Data set

We have collected a data set of DBT with the prototype DBT system for development of image reconstruction and lesion detection techniques for DBT. The subjects were recruited with Institutional Review Board (IRB) approval and written informed consent. Eligible subjects were women who had undergone diagnostic work up for a suspicious finding by screening or clinical examinations. Two-view DBTs, i.e., craniocaudal (CC) and mediolateral oblique (MLO) views, of the breast with the lesion were acquired. For the majority of the DBT scans, the system was set to acquire 21 PVs in 3° increments, with a total tomographic angle of 60° (referred to as wide-angle scan). For a small subset of the subjects, the system was set to acquire 17 projections in 1° increments with a total tomographic angle of 16° (referred to as narrow-angle scan). For the development of the MAR technique, we retrospectively searched our DBT database of about 800 cases and found 41 breasts with biopsy clips. Ten breasts with 9 CC views and 10 MLO views were used for development of the MAR methods; the only selection criterion was that together they contained the different types of biopsy clips in our data set. The training set was selected before the narrow-angle subset was obtained so that all training views were wide-

Author Manuscript Author Manuscript Author Manuscript Author Manuscript

angle scans. The other 31 breasts with biopsy clips, including 28 acquired with wide angle and 3 acquired with narrow angle, were independent of the training cases and used for performance testing. Of the 31 breasts, two did not have MLO view and the clips were out of the field of view on one CC view and one MLO view, resulting in a total of 58 (= 31*2 − 4) DBT views. All 4 missing views were from the wide angle data set so that there were 52 wide-angle views and 6 narrow-angle views. Two breasts (4 views) in the training set and one breast (2)views) in the test set had both a small core biopsy clip and a cluster of large lumpectomy clips. Table 1 shows the number of breasts, the number of DBT views, and the number of DBT views containing each type of clips. Because the data set was relatively small and we did not observe differences in MAR for the CC and MLO views, the two views were treated the same in all processing steps and analyses.

C. Metal Artifacts in DBT

When a breast with a metallic clip marker undergoes x-ray imaging, the x-rays intersecting the metallic clip are highly attenuated so that the pixels of the projected metal clip images on the detector have low exposure. Fig. 2 illustrates the ray paths intersecting a metallic clip in the breast for three PVs. The hatched regions are the conical artifact regions in which the ray paths from each of the source position intersect and are attenuated by the object. During reconstruction, because the location of the metallic clip in the reconstruction volume is not known, the total attenuation (for backprojection-type reconstruction) or the total attenuation error between the calculated value and the detected value (for iterative reconstruction) is uniformly assigned to every voxel along the ray path for a given detector bin. This causes overestimation of the attenuation at the voxels that contained breast tissue along the ray and underestimation of the attenuation of the voxels containing the clip. Because a small number of PVs are acquired in a limited angular range for a DBT scan, the voxel value errors in the artifact region cannot be compensated by updating from other PVs, especially the lack of PVs at large angles (e.g., perpendicular) relative to the PV that causes the artifacts. The errors in the estimated voxel values lead to strong interplane and inplane metal artifacts in the reconstruction volume. As illustrated in Fig. 2, the black region below and above the metallic object, where the conical artifact regions subtended by the object at the x-ray source from all available PVs overlap, cannot be updated correctly by any ray path that does not intersect the metal object in a limited-angle tomography geometry. The voxels in the overlap regions therefore do not obtain correct tissue information for updating and maintain the overestimated values at the end of reconstruction. Away from this region, the voxels in the artifact region of some PVs may be partially compensated from the unaffected detector bins outside the artifact regions of the other PVs. The farther the voxels are from the overlap region, the more likely they will be updated with ray paths outside the artifact regions of some PVs and the smaller the overestimation errors are. The intensity of the metal artifacts therefore decreases as the distances from the focal plane of the object increases. The artifacts appear as repeating images of the object on reconstructed slices above and below the focal plane, where the slice intersects with the artifact region of each PV. The artifact images increasingly separate from one another along the scan direction of the x-ray source as the distance of the slice from the focal plane increases. An example of the interplane metal artifacts from three metal clips in a breast is shown in the left column of Fig. 3. The artifacts extend below and above the actual depth of the clips and each appeared in a typical “X”-

Author Manuscript Author Manuscript Author Manuscript Author Manuscript

shape on the Y-Z plane due to the angular sweep of x-ray source while the artifacts in the X-Z plane are only slightly angulated due to the cone beam geometry. The metal artifacts will overlap with the breast tissue structures and may obscure subtle lesions such as microcalcifications or masses, which not only degrade the DBT image quality but also interfere with breast cancer detection and diagnosis.

As shown in Fig. 2 and Fig. 3, the errors in the estimation of the attenuation along the x-ray path through the stack of reconstruction slices spread the artifacts far beyond the voxels containing the marker, which makes it difficult to regularize the voxel values of the artifact regions in the reconstructed volume using geometric features. Our approach is to reduce the attenuation of the metal markers on the individual PVs by an iterative diffusion method before reconstruction. The locations of the markers are automatically detected and labeled on the PVs to provide a map for replacing the high-contrast objects with the low-frequency tissue background gray levels estimated by diffusion inpainting from the surrounding local region.

D. Automated Metallic Marker Detection in Projection Images

Our automated metallic marker detection method includes three stages: (1) preprocessing; (2) segmentation of metallic marker candidates; (3) FP reduction using voting technique. The detail of each stage will be described below.

D.1 Preprocessing—The PVs output from the DBT system are stored as raw images in which the pixel values are linearly proportional to x-ray intensity at the detector. The logarithmic transform is first applied to the raw PVs, which is the same operation as SART without MAR. Therefore, all subsequent image processing including DBT reconstruction with or without MAR is performed on the logarithmic- transformed PVs and they will simply be referred to as PVs in the following.

An automated breast boundary detection algorithm for mammograms developed in our laboratory is adapted to detect the two-dimensional (2D) breast boundary on each PV (Zhang *et al* 2007, Wu *et al* 2010). The values of the pixels outside the breast region are set as zero. Further steps are only applied to the segmented breast region to reduce computation time.

The difference-image technique is used to remove the structured background and facilitate the detection of signals (Chan *et al* 1987, Chan *et al* 1995, Ge *et al* 2006). The PV is smoothed using a low-pass filter to estimate the background gray levels. The low-pass filtered image is then subtracted from the unfiltered image to remove the structured background while maintaining the higher-frequency details. The subtracted image has relatively flat background gray levels and facilitates the separation of the signal and background pixels. We experimentally chose a 51×51 box filter to remove the breast background. The difference image is used for the following metallic clip marker detection.

D.2 Segmentation of Metallic Marker Candidates—The histogram of the difference image is analyzed. The pixels with values below the mean plus one standard deviation of the pixel values within the breast region are classified as the initial background pixel candidates.

Author Manuscript Author Manuscript Author Manuscript Author Manuscript

The high pixel values in the difference image above an iteratively adjusted global threshold value are used as the feature to select the seed points of signal candidates. Each signal candidate is segmented by local signal region growing guided by the local contrast-to-noise ratio (CNR) around the seed point as follows. The local root-mean-square noise is estimated from the neighboring background pixels in a region-of-interest (ROI) centered at the seed point but excluding all pixels above the global threshold. The ROI size is adaptively adjusted to contain at least 400 background pixels, which we found to be large enough for estimating the background root-mean-square noise without excessive computation time. For a candidate pixel that is connected to the seed point based on 8-connectivity, if the calculated CNR of the pixel is above a pre-selected CNR threshold criterion, the pixel is considered a part of the signal candidate. A grown signal having an area within a predefined range is considered to be an effective signal candidate. From the training set of projection images containing metallic clip markers of various sizes and shapes and knowledge about the detection of microcalcifications (Chan *et al* 1987, Chan *et al* 1995, Chan *et al* 1998, Ge *et al* 2007b, Sahiner *et al* 2012, Samala *et al* 2015) and metallic objects (Hadjiiski *et al* 2015, Sengupta *et al* 2017) from our previous studies, we experimentally chose the CNR threshold to be 6.0 and the size range to be between 30 and 2500 pixels for the signal candidates. The minimum object size of 30 pixels, corresponding to a circular object of about 6 pixels (0.6 mm) in diameter, was chosen because it is smaller than the sizes of microclips but much larger than microcalcifications. The maximum size of 2500 pixels, which is about 2 to 3 times the size of a large lumpectomy clip, was chosen to take into consideration that some clips can overlap in the projections and merge into a larger object. The size threshold, together with a CNR threshold of 6 that is greater than the CNR of most microcalcifications, will exclude clinically significant microcalcifications from being detected as metal objects. This signal extraction procedure is performed iteratively using adaptively adjusted global threshold value until the number of signal candidates are within a predefined range between 1 and 20. After the detection step of the signal candidates is terminated, the same signal region growing algorithm is applied to each of the detected signal candidates to refine the segmentation of the signal candidate.

D.3 False Positive Reduction Using Voting Technique—After the signal detection procedure described above has been performed in all PVs, a voting technique is applied to the segmentation results from the PVs at all angles to reduce the FPs. A binary image is first generated from the segmented signal for each PV. The signal pixels are labeled as 1 and other pixels are labeled as 0. The binary images are then backprojected to the reconstruction volume following the DBT geometry. If a ray from a nonzero pixel on the binary image at one projection angle passes through a voxel in the reconstruction volume, the voxel receives one vote from the PV at the corresponding angle. The voxels with total votes greater than a threshold are treated as seed points of metallic clip markers and a connection operator is used to label all connected voxels that satisfy the threshold criterion. The threshold is adaptively determined for each voxel as follows. The boundary of the field of view of each PV in the reconstructed volume can be calculated from the known imaging geometry and the depth of each slice (Lu *et al* 2013a). For a given voxel, the maximum number of PVs that can contribute a ray intersecting the voxel can therefore be determined from the location of the voxel in the reconstructed volume. The threshold is chosen to be this maximum number

Author Manuscript Author Manuscript Author Manuscript Author Manuscript

of PVs minus 1 to accommodate potential numerical error of ray-tracing. The connected voxels are considered a volume of interest (VOI) of a metallic marker and are labeled as 1 if the VOI size is greater than a minimum number of voxels, which is chosen as the same as the minimum detected signal size (i.e., 30 pixels) on a PV. After labeling all metallic marker candidates, the remaining voxels are labeled as 0.

After the segmented VOIs of the metallic marker are generated, the binary reconstruction volume is forward-projected to the 2D binary image at each projection angle. The detected signal candidates in the 2D binary image that do not intersect any x-rays passing through the segmented VOIs are removed as FPs by labeling the corresponding pixels as 0. The binary image with the remaining detected signal candidates labeled as 1 is defined as the metallic clip marker location map for the PV at that angle.

E. Diffusion Method

We developed a diffusion-based method to estimate the missing tissue background in the marker regions on the PVs. The purpose is to compensate for the reduced x-ray intensity in the marker region using the neighboring background information before reconstruction.

Let Ω denote a binary mask region with pixels labeled as 1 in the generated metallic clip marker location map for a given projection image S and D the domain of S. To reduce the metal artifacts, we estimate the expected pixel values for tissue in the region Ω assuming that the metal clip displaced tissue of pixel values similar to those in the neighboring region of Ω. For the voxels of the artifact regions in the reconstruction volume, they may be affected by a few of the PVs and still have true projection information from other PVs. To preserve the image details that may be reconstructed from other PVs visible to the voxels in the artifact region, the compensation in the PVs only needs to approximate the low-frequency background. The following diffusion-based method is designed to estimate the low-frequency background in Ω using the information from the neighboring region of Ω in $D\backslash\Omega$. We define the projection operator $\boldsymbol{P}_\Omega$ as

$$\boldsymbol{P}_\Omega S(k)=\begin{cases} S(k) & k\in\Omega \\ 0 & k\in D\backslash\Omega \end{cases}, \quad (2)$$

where k is the index of a voxel in D. The operation $\boldsymbol{P}_\Omega S(k)$ generates a temporary image that takes the pixel values from an image $S(k)$ under the binary mask region Ω while setting all pixels outside Ω (i.e., $D\backslash\Omega$) to zero.

With an iterative diffusion operation, the image S_j at the j-th iteration of diffusion is given by

$$S_j=(\boldsymbol{I}-\boldsymbol{P}_\Omega)S_{j-1}+\boldsymbol{P}_\Omega\left(F**S_{j-1}\right), \quad (3)$$

where $\boldsymbol{I}$ is the identity operator, F is a 2D low-pass filter. ** denotes 2D convolution. J denotes the number of iterations chosen for generating the inpainted image, j=1,…,J.

Author Manuscript Author Manuscript Author Manuscript Author Manuscript

The first term in Eq. (3) takes the image from the $(j-1)$th iteration $\boldsymbol{I}S_{j-1} = S_{j-1}$ (because $\boldsymbol{I}$ is an identity operator) and subtracts it with a temporary image $\boldsymbol{P}_{\Omega}(S_{j-1})$, which results in an image with zeros in the mask region Ω and pixel values identical to those of S_{j-1} outside the mask because $\boldsymbol{P}_{\Omega}(S_{j-1})$ has pixel values of S_{j-1} inside the mask and 0 for all pixels outside the mask as defined by Eq. (2). The second term $\boldsymbol{P}_{\Omega}(F^{**} S_{j-1})$ is a temporary image that has pixel values from the diffused image $F^{**} S_{j-1}$ inside the mask region and zeros outside the mask. Summation of the two terms yields the image S_j, which has the mask region filled with the diffused pixel values while the pixel values outside the mask region remain exactly the same as those in S_{j-1}. This iterative process is initialized at $j=1$ by setting $S_0 = (\boldsymbol{I} - \boldsymbol{P}_{\Omega})S$, which is the original projection having the high contrast pixels in the mask region removed. It can be seen that this diffusion process preserves the original pixel values obtained from $S_0 = (\boldsymbol{I} - \boldsymbol{P}_{\Omega})S$ outside the mask region, no noise or blurring is imposed regardless of the number of iterations, while the pixels inside the mask region will be iteratively updated with the diffused pixel values from the low-pass filtered image.

We applied this iterative diffusion process to each of the PVs. For each PV, at the end of J iterations, we obtained a projection image S_J that has its original pixel values outside the mask region, $D\backslash\Omega$, while the pixels in Ω are inpainted with the values obtained from the diffused low-frequency tissue background. This set of PVs that have the metal objects removed and the “holes” compensated with approximate tissue values are used for DBT reconstruction.

To show the clip in the reconstructed DBT volume so that radiologists can identify the biopsy site, the voxels at the location of the metal clip as determined by the voting technique are re-painted with high voxel values at the end of reconstruction with MAR.

F. Study conditions

We evaluated the MAR method by reconstructing DBT images with and without MAR. The proposed method is independent of the reconstruction technique because it is applied to the PV images. We used SART (Lu *et al* 2010) in which the imaged volume was initialized with a constant of 0.5 and a relaxation parameter of 0.5 was used for the first iteration and 0.3 for the subsequent iterations. Based on our experiments, we observed that the choice of the 2D low-pass filter F and the kernel size for diffusing the image S_{j-1} in Eq. (3) is not critical but small kernels will require more diffusion iterations. We chose the low-pass filter to be a box filter with a kernel size of 41X41 pixels. The diffusion process was terminated automatically when further iterations did not cause substantial changes in the diffused region Ω. We experimentally chose the stopping criterion to be a change of less than 1% in the average gray level in Ω.

G. Performance evaluation

The performance of the MAR was evaluated visually on the reconstructed DBT images because the residual artifacts can be seen easily in the breast tissue background but it is not easy to develop an automated system for detecting and scoring reliably residual artifacts that may have a variety of shapes and contrasts. The metal artifact was considered successfully removed from the reconstructed DBT volume (CC or MLO view) only if the metal marker

Author Manuscript Author Manuscript Author Manuscript Author Manuscript

was detected and filled by diffusion on all PVs of that DBT view. False negative detection in any of the PVs would leave residual artifact in the reconstructed volume although the intensity of the artifact decreased as the metal marker was removed from increasing number of PVs.

The focus of the current study is to reduce the artifacts from metal markers in the breast. Similar to metal markers, large dense benign calcifications also cause interplane and inplane artifacts. The removal of these artifacts has the same positive effect on image quality. However, because our data set was not collected with the dense benign calcifications as objects of interest, we did not have enough samples to evaluate the performance of our MAR method in removing the calcification artifacts. We therefore scored the removal of calcification artifacts as FPs.

III. RESULTS

Table 1 summarizes the performance of our MAR method. The success rate was counted separately for the two types of metal markers because they had very different characteristics. The proposed MAR method is effective in removing the metal artifacts for the small biopsy microclips of any shape. Figure 4 shows examples of core biopsy clips of various shapes. The success rate of MAR for microclips reached 97.2% (35 of 36 views) in the test set. However, the success rate of MAR for the large post-lumpectomy markers was low at 66.7% (16 of 24 views). As shown in the examples in Fig. 3 and Fig. 5, multiple large markers are often placed at a lumpectomy site. The projected multiple marker images may overlap one another on the PVs, resulting in a wide range of sizes and shapes of the target objects to be detected. The large number of markers on each PV also increases the chance that some of the markers may be missed on some of the PVs, causing residual artifacts and failure. Each of the 8 DBT volumes that failed contained 7 to 19 large lumpectomy markers. The metal artifacts were partially removed in all 8 volumes and the majority of the remaining artifacts were caused by clusters of overlapping markers that the detection failed in some of the PVs. However, even if the MAR algorithms failed partially, the artifacts were still substantially reduced as shown in the example in Fig. 5. Figure 3 and Fig. 6 show two examples in which all the large clips were successfully removed by the MAR method and the spiculated tissue or microcalcifications at the biopsy site became easily visible. The 6 views of narrow-angle DBTs included 4 views with small core biopsy clips and 2 views with large post-lumpectomy markers; MAR was successful in all 6 views.

The voting technique eliminated the FPs that were detected at random locations in the PVs. All FPs that remained in the reconstructed DBT volume were dense benign calcifications. The FP rate was therefore related to the number of large benign calcifications present in the data set. The locations of the benign calcifications were re-painted in the DBT slices after reconstruction for radiologists' information. An example can be seen in Fig. 4(c).

IV. DISCUSSION

Metal artifact reduction is important to improve the image quality of DBT reconstruction when metallic clip exists in the breast. In particular, the biopsy sites are often the location of

Author Manuscript Author Manuscript Author Manuscript Author Manuscript

previous cancer where the chance of recurrence is high. The metal artifacts obscure the neighboring tissue in follow-up examinations and may delay early diagnosis of recurring breast cancer. As seen in the examples in Fig. 3 and Fig. 6, the visibility and the features of the spiculated structures and microcalcifications in the artifact regions are obscured or distorted by the shadows of the metal clips. With the proposed method, the interplane and inplane metal artifacts are reduced to a level that is not apparent in the reconstructed slices. The visibility of important details along the ray paths is restored. The diffusion-based MAR method reduces the metal artifacts while preserving the image information in the surrounding regions.

The physical position of metallic clips is unknown for a given DBT. One effective way to estimate the clip locations is to identify low x-ray intensity pixels from highly attenuated objects on the PVs. The geometric correlation of an object among PVs at different projection angles is another important piece of information to determine the possible region of metallic clips. We developed an automated clip detection method that exploits the contrast feature of the high-attenuation metallic objects on x-ray projections. The adaptive thresholding and region growing techniques are found to be useful in detecting and segmenting the potential metallic clip marker regions. However, in some cases, the projected metallic clip regions may be highly distorted in size and shape, such as those with overlapping clusters of clips, and become false negatives while dense fibrous tissue or dense large calcifications may be detected as potential signals. Making use of the geometric correlation of the true objects projected to the PVs at different angles, we back-project the detected regions from different PVs to the imaged volume to estimate the convergence locations of the potential dense objects in 3D. A voting technique is designed to identify locations that have high likelihood of object convergence. We found that the convergence votes are useful for differentiating true and FP candidates when the FPs are caused by fibrous tissue that do not have consistent density, size and shape across the different projections. A voting threshold with low tolerance leads to high specificity of the detection algorithm.

Our results indicate that the proposed MAR method can be used to remove artifacts caused by large dense calcifications. The detection of large dense calcifications is similar to detection of metal clips. If they are large and dense enough to pass the prescreening stage in multiple projections, the voting technique will not exclude them because they are true objects with high geometric correlations. Removing artifacts caused by large dense calcifications is desirable because it also improves image quality of DBT. It will be of interest to conduct a follow-up study to evaluate the performance of the MAR method in removing the large calcification artifacts and preserving the shapes of the calcifications when a larger data set containing these calcifications is available.

The metallic clip markers obscure the tissue information along the x-rays corresponding to the highly attenuated region in the projections and cause undetermined voxel regions in the reconstructed volume. For natural scene images, inpainting technique is used to estimate the missing information in an image and geometric-structure-driven algorithms are developed previously. However, the overlapping of breast tissue may cause discontinuity of anatomical structures in the PVs of the breast and the hypothesis of conventional inpainting methods may not be satisfied. As a result, we chose to only compensate for the low-frequency

Author Manuscript Author Manuscript Author Manuscript Author Manuscript

background using neighboring pixel information in a PV. This approach works well based on the imaging geometry of DBT. The voxels in the reconstructed volume that are affected by metallic clip markers in one or more projection angles may be unaffected at other projection angles (hatched regions in Fig. 2). Therefore, although only the low-frequency components at the angles where the projected voxel information is lost are compensated for, the high-frequency details may be reconstructed from the projections at the angles where the voxels intersect with ray paths that are not obstructed by the dense object. Only the black regions shown in Fig. 2 just above and below the dense object are void of information from all PVs. Because the boundary of the object (e.g., the top and bottom surfaces of the spherical object in Fig. 2) cannot be determined in these regions, they are filled with high voxel values in the reconstructed volume, resulting in the elongated shape of the re-painted regions seen in the X-Z and Y-Z cross-sections of the clips in the right column of Fig. 3. The elongation of the black regions (or the re-painted regions) increases as the scan angle of the DBT acquisition decreases.

Our current MAR algorithm has limitations. Its performance in removal of large clusters of overlapping post-lumpectomy markers is relatively low. The major problem is the large variabilities in the size and shape of the target objects that lead to false negatives from pieces of the cluster. With the multiple PVs in the DBT scan, it becomes difficult to achieve perfect detection and inpainting in all PVs. One potential method to reduce the false negatives is to use the locations of VOIs with high convergence votes, but below the threshold, in the backward-projected binary volume as a guide to conduct a second-stage detection. The VOIs may be forward-projected to the PVs that do not contribute votes to identify regions of interest for a local search of possible target objects on these PVs. Furthermore, as our training set is small, the chosen parameters may not be robust enough for unknown cases such as those in the independent test set. We expect that the MAR method and parameters can be further improved to more accurately detect clusters of large metal markers when a larger training set is available. Nevertheless, even if the artifact is not completely removed, cleaning up a high- attenuation object in any PVs before reconstruction will still reduce the intensity of the artifact in the reconstructed volume to some extent.

Another limitation is the small number of breasts with metallic clips that can be collected, as only a small fraction of patients has undergone previous biopsy and have biopsy clips left in the breast, especially cases with recurring subtle cancer in the artifact regions. As a result, we cannot study a variety of issues associated with MAR such as the dependence of its performance on DBT scan geometry, whether the MAR restored image information can be proven to be clinically significant in cancer diagnosis, or whether repainting the removed dense object on the output DBT slices may distort its shape and affect diagnosis. Nevertheless, our approach of replacing the high-contrast object in the projections with diffused low-frequency background pixel values before reconstruction makes our MAR method less likely to be dependent on DBT scan geometry. Removing the high-contrast object artifacts improves the image quality and reduces radiologists' concern that important information may be obscured by the artifacts, regardless of whether the improvement actually increases diagnostic accuracy. The examples in Fig. 4 with microclips of various shapes also show that our algorithm is capable of repainting object shapes with recognizable details. Ideally, researchers can develop computer models to generate a large set of breast

Author Manuscript Author Manuscript Author Manuscript Author Manuscript

phantoms with realistic breast-tissue-mimicking parenchymal patterns, embedded with subtle microcalcifications and spiculated masses as well as biopsy clips of various shapes at any desired locations, and produce projections at any chosen DBT scan geometries. Such phantom models will facilitate all kinds of studies for development of reconstruction, image quality improvement and lesion detection techniques for DBT, including the issues of MAR mentioned above, providing perfect ground truth for quantitative assessments without the challenges and costs of collecting patient cases. Simulated phantom images will also be useful for quantitative assessment of the accuracy of the repainted object and the tissue background by the MAR method. However, to our knowledge, such phantom models are still work in progress by researchers after years of developmental effort. The above studies will have to be pursued by interested researchers who have access to such models in the future.

V. CONCLUSION

In this study, we proposed a metal artifact reduction method for DBT reconstruction. An automated algorithm was developed to detect the highly attenuated regions from metallic clip markers in the projection images before reconstruction. A voting technique was designed for FP reduction and generation of a marker location map at each projection. A diffusion-based in-painting method was applied to each projection to compensate for the low-frequency background labeled by the marker location maps while preserving the pixel values in the surrounding regions. The compensated projections are used for DBT reconstruction. The results demonstrated that the proposed diffusion-based MAR method can restore the visibility of tissue structures and image information obscured by the metal artifacts. Reducing the metal artifacts in DBT can potentially improve detection and assessment of subtle breast lesions, which is especially important for early detection of cancer recurrence near the previous biopsy site.

Acknowledgments

This work is supported by National Institutes of Health award number RO1 CA151443.

References

Abdoli M, Ay MR, Ahmadian A, Dierckx R, Zaidi H. Reduction of dental filling metallic artifacts in CT-based attenuation correction of PET data using weighted virtual sinograms optimized by a genetic algorithm. Medical Physics. 2010; 37:6166–77. [PubMed: 21302773]

Abdoli M, Dierckx R, Zaidi H. Metal artifact reduction strategies for improved attenuation correction in hybrid PET/CT imaging. Medical Physics. 2012; 39:3343–60. [PubMed: 22755716]

Badea C, Kolitsi Z, Pallikarakis N. A wavelet-based method for removal of out-of-plane structures in digital tomosynthesis. Computerized Medical Imaging and Graphics. 1998; 22:309–15. [PubMed: 9840661]

Bal M, Spies L. Metal artifact reduction in CT using tissue-class modeling and adaptive prefiltering. Medical Physics. 2006; 33:2852–9. [PubMed: 16964861]

Bazalova M, Beaulieu L, Palefsky S, Verhaegen F. Correction of CT artifacts and its influence on Monte Carlo dose calculations. Medical Physics. 2007; 34:2119–32. [PubMed: 17654915]

Bernardi D, Macaskill P, Pellegrini M, Valentini M, Fantò C, Ostillio L, Tuttobene P, Luparia A, Houssami N. Breast cancer screening with tomosynthesis (3D mammography) with acquired or synthetic 2D mammography compared with 2D mammography alone (STORM-2): a population-based prospective study. Lancet Oncololgy. 2016; 17:1105–13.

Author Manuscript Author Manuscript Author Manuscript Author Manuscript

Boas FE, Fleischmann D. Evaluation of Two Iterative Techniques for Reducing Metal Artifacts in Computed Tomography. Radiology. 2011; 259:894–902. [PubMed: 21357521]

Chakraborty DP, Yester MV, Barnes GT, Lakshminarayanan AV. Selfmasking subtraction tomosynthesis. Radiology. 1984; 150:225–9. [PubMed: 6359264]

Chan H-P, Doi K, Galhotra S, Vyborny CJ, MacMahon H, Jokich PM. Image feature analysis and computer-aided diagnosis in digital radiography. 1. Automated detection of microcalcifications in mammography. Medical Physics. 1987; 14:538–48. [PubMed: 3626993]

Chan H-P, Goodsitt MM, Helvie MA, Zelakiewicz S, Schmitz A, Noroozian M, Paramagul C, Roubidoux MA, Nees AV, Neal CH, Carson P, Lu Y, Hadjiiski L, Wei J. Digital Breast Tomosynthesis: Observer Performance of Clustered Microcalcification Detection on Breast Phantom Images Acquired with an Experimental System Using Variable Scan Angles, Angular Increments, and Number of Projection Views. Radiology. 2014; 273:675–85. [PubMed: 25007048]

Chan H-P, Lo SCB, Sahiner B, Lam KL, Helvie MA. Computer-aided detection of mammographic microcalcifications: Pattern recognition with an artificial neural network. Medical Physics. 1995; 22:1555–67. [PubMed: 8551980]

Chan H-P, Sahiner B, Lam KL, Petrick N, Helvie MA, Goodsitt MM, Adler DD. Computerized analysis of mammographic microcalcifications in morphological and texture feature space. Medical Physics. 1998; 25:2007–19. [PubMed: 9800710]

Ciatto S, Houssami N, Bernardi D, Caumo F, Pellegrini M, Brunelli S, Tuttobene P, Bricolo P, Fanto C, Valentini M, Montemezzi S, Macaskill P. Integration of 3D digital mammography with tomosynthesis for population breast-cancer screening (STORM): a prospective comparison study. Lancet Oncology. 2013; 14:583–9. [PubMed: 23623721]

Claus BEH, Eberhard JW. A new method for 3D reconstruction in digital tomosynthesis. Proc SPIE. 2002; 4684:814–24.

Conant EF, Beaber EF, Sprague BL, Herschorn SD, Weaver DL, Onega T, Tosteson ANA, McCarthy AM, Poplack SP, Haas JS, Armstrong K, Schnall MD, Barlow WE. Consortium P. Breast cancer screening using tomosynthesis in combination with digital mammography compared to digital mammography alone: a cohort study within the PROSPR consortium. Breast Cancer Research and Treatment. 2016; 156:109–16. [PubMed: 26931450]

De Man B, Nuyts J, Dupont P, Marchal G, Suetens P. Reduction of metal streak artifacts in x-ray computed tomography using a transmission maximum a posteriori algorithm. IEEE Transactions on Nuclear Science. 2000; 47:977–81.

Durand MA, Haas BM, Yao XP, Geisel JL, Raghu M, Hooley RJ, Horvath LJ, Philpotts LE. Early Clinical Experience with Digital Breast Tomosynthesis for Screening Mammography. Radiology. 2015; 274:85–92. [PubMed: 25188431]

Friedewald SM, Rafferty EA, Rose SL, Durand MA, Plecha DM, Greenberg JS, Hayes MK, Copit DS, Carlson KL, Cink TM, Barke LD, Greer LN, Miller DP, Conant EF. Breast Cancer Screening Using Tomosynthesis in Combination With Digital Mammography. JAMA-Journal of the American Medical Association. 2014; 311:2499–507.

Ge J, Chan H-P, Zhang Y, Sahiner B, Wei J, Hadjiiski LM, Zhou C. Digital tomosynthesis mammography: Intra- and interplane artifact reduction for high-contrast objects on reconstructed slices using a priori 3D geometrical information. Proc SPIE. 2007a; 6512:65124Q.

Ge J, Hadjiiski LM, Sahiner B, Wei J, Helvie MA, Zhou C, Chan H-P. Computer-aided detection system for clustered microcalcifications: comparison of performance on full-field digital mammograms and digitized screen-film mammograms. Physics in Medicine and Biology. 2007b; 52:981–1000. [PubMed: 17264365]

Ge J, Sahiner B, Hadjiiski LM, Chan H-P, Wei J, Helvie MA, Zhou C. Computer aided detection of clusters of microcalcifications on full field digital mammograms. Medical Physics. 2006; 33:2975–88. [PubMed: 16964876]

Gilbert FJ, Tucker L, Young KC. Digital breast tomosynthesis (DBT): a review of the evidence for use as a screening tool. Clinical Radiology. 2016; 71:141–50. [PubMed: 26707815]

Gjesteby L, Man BD, Jin Y, Paganetti H, Verburg J, Giantsoudi D, Wang G. Metal Artifact Reduction in CT: Where Are We After Four Decades? IEEE Access. 2016; 4:5826–49.

Author Manuscript Author Manuscript Author Manuscript Author Manuscript

Glover GH, Pelc NJ. An algorithm for the reduction of metal clip artifacts in CT reconstructions. Medical Physics. 1981; 8:799–807. [PubMed: 7322078]

Goodsitt MM, Chan H-P, Schmitz A, Zelakiewicz S, Telang S, Hadjiiski L, Watcharotone K, Helvie MA, Paramagul C, Christodoulou E, Larson SC, Carson PL. Digital breast tomosynthesis: studies of the effects of acquisition geometry on contrast-to-noise ratio and observer preference of low-contrast objects in breast phantom images. Physics in Medicine and Biology. 2014; 59:5883–902. [PubMed: 25211509]

Hadjiiski L, Marentis TC, Chaudhury AR, Rondon L, Chronis N, Chan H-P. Computer aided detection of surgical retained foreign object for prevention. Medical Physics. 2015; 42:1213–22. [PubMed: 25735276]

Kalender WA, Hebel R, Ebersberger J. Reduction of CT artifacts caused by metallic implants. Radiology. 1987; 164:576–7. [PubMed: 3602406]

Kopans DB. Novel approaches and newer imaging modalities. Course 815: Problem-solving Breast Imaging. RSNA Program Book. 2001; 2001:97.

Levakhina YM, Muller J, Duschka RL, Vogt F, Barkhausen J, Buzug TM. Weighted simultaneous algebraic reconstruction technique for tomosynthesis imaging of objects with high-attenuation features. Medical Physics. 2013; 40:031106. [PubMed: 23464286]

Lewitt RM. Processing of incomplete measurement data in computed tomography. Medical Physics. 1979; 6:412–7. [PubMed: 492075]

Lu Y, Chan H-P, Wei J, Hadjiiski L, Samala R. Multiscale Bilateral Filtering for Improving Image Quality in Digital Breast Tomosynthesis. Medical Physics. 2015; 42:182–95. [PubMed: 25563259]

Lu Y, Chan H-P, Wei J, Hadjiiski LM. Selective-diffusion regularization for enhancement of microcalcifications in digital breast tomosynthesis reconstruction. Medical Physics. 2010; 37:6003–14. [PubMed: 21158312]

Lu Y, Chan H-P, Wei J, Hadjiiski LM. A diffusion-based truncated projection artifact reduction method for iterative digital breast tomosynthesis reconstruction. Physics in Medicine and Biology. 2013a; 58:569–87. [PubMed: 23318346]

Lu Y, Chan H-P, Wei J, Hadjiiski LM, Samala RK. Improving Image Quality for Digital Breast Tomosynthesis: Automatic Detection and Inpainting Method for Metal Artifact Reduction. RSNA Program. 2013b; 2013:SSM21–06.

Mahnken AH, Raupach R, Wildberger JE, Jung B, Heussen N, Flohr TG, Gunther RW, Schaller S. A new algorithm for metal artifact reduction in computed tomography - In vitro and in vivo evaluation after total hip replacement. Investigative Radiology. 2003; 38:769–75. [PubMed: 14627894]

Mehranian A, Ay MR, Rahmim A, Zaidi H. Sparsity Constrained Sinogram Inpainting for Metal Artifact Reduction in X-ray Computed Tomography. Proceedings IEEE Nuclear Science Symposium and Medical Imaging Conference. 2011; 2011:3694–9.

Niklason LT, Christian BT, Niklason LE, Kopans DB, Castleberry DE, Opsahl-Ong BH, Landberg CE, Slanetz PJ, Giardino AA, Moore R, Albagli D, DeJule MC, Fitzgerald FC, Fobare DF, Giambattista BW, Kwasnick RF, Liu J, Lubowski SJ, Possin GE, Richotte JF, Wei CY, Wirth RF. Digital tomosynthesis in breast imaging. Radiology. 1997; 205:399–406. [PubMed: 9356620]

Nuyts, J., Stroobants, S. Reduction of attenuation correction artifacts in PET-CT. 2005 IEEE Nuclear Science Symposium Conference Record; 2005. p. 1895-9.

Rose SL, Tidwell AL, Bujnoch LJ, Kushwaha AC, Nordmann AS, Sexton R. Implementation of Breast Tomosynthesis in a Routine Screening Practice: An Observational Study. American Journal of Roentgenology. 2013; 200:1401–8. [PubMed: 23701081]

Sahiner B, Chan H-P, Hadjiiski LM, Helvie MA, Wei J, Zhou C, Lu Y. Computer-aided detection of clustered microcalcifications in digital breast tomosynthesis: A 3D approach. Medical Physics. 2012; 39:28–39. [PubMed: 22225272]

Samala RK, Chan H-P, Lu Y, Hadjiiski LM, Wei J, Helvie MA. Computer-aided Detection System for Clustered Microcalcifications in Digital Breast Tomosynthesis using Joint Information from Volumetric and Planar Projection Images. Physics in Medicine and Biology. 2015:608457–79.

Sechopoulos I. A review of breast tomosynthesis. Part I. The image acquisition process. Medical Physics. 2013; 40:014301. [PubMed: 23298126]

Author Manuscript Author Manuscript Author Manuscript Author Manuscript

Sengupta A, Hadjiiski L, Chan H-P, Cha K, Chronis N, Marentis TC. Computer-aided detection of retained surgical needles from postoperative radiographs. Medical Physics. 2017; 44:180–91. [PubMed: 28044343]

Sharpe RE, Venkataraman S, Phillips J, Dialani V, Fein-Zachary VJ, Prakash S, Slanetz PJ, Mehta TS. Increased Cancer Detection Rate and Variations in the Recall Rate Resulting from Implementation of 3D Digital Breast Tomosynthesis into a Population-based Screening Program. Radiology. 2016; 278:698–706. [PubMed: 26458206]

Skaane P, Bandos AI, Gullien R, Eben EB, Ekseth U, Haakenaasen U, Izadi M, Jebsen IN, Jahr G, Krager M, Hofvind S. Prospective trial comparing full-field digital mammography (FFDM) versus combined FFDM and tomosynthesis in a population-based screening programme using independent double reading with arbitration. European Radiology. 2013a; 23:2061–71. [PubMed: 23553585]

Skaane P, Bandos AI, Gullien R, Eben EB, Ekseth U, Haakenaasen U, Izadi M, Jebsen IN, Jahr G, Krager M, Niklason LT, Hofvind S, Gur D. Comparison of Digital Mammography Alone and Digital Mammography Plus Tomosynthesis in a Population-based Screening Program. Radiology. 2013b; 267:47–56. [PubMed: 23297332]

Veldkamp WJH, Joemai RMS, van der Molen AJ, Geleijns J. Development and validation of segmentation and interpolation techniques in sinograms for metal artifact suppression in CT. Medical Physics. 2010; 37:620–8. [PubMed: 20229871]

Verburg JM, Seco J. CT metal artifact reduction method correcting for beam hardening and missing projections. Physics in Medicine and Biology. 2012; 57:2803–18. [PubMed: 22510753]

Wicklein J, Jerebko A, Ritschl L, Mertelmeier T. Metal and calcification artifact reduction for digital breast tomosynthesis. Proc SPIE. 2017; 10132:1013224.

Wu T, Moore RH, Kopans DB. Voting strategy for artifact reduction in digital breast tomosynthesis. Medical Physics. 2006; 33:2461–71. [PubMed: 16898449]

Wu YT, Zhou C, Chan H-P, Paramagul C, Hadjiiski LM, Daly CP, Douglas JA, Zhang YH, Sahiner B, Shi JZ, Wei J. Dynamic multiple thresholding breast boundary detection algorithm for mammograms. Medical Physics. 2010; 37:391–401. [PubMed: 20175501]

Zhang Y, Chan H-P, Sahiner B, Wei J, Goodsitt MM, Hadjiiski LM, Ge J, Zhou C. A comparative study of limited-angle cone-beam reconstruction methods for breast tomosynthesis. Medical Physics. 2006; 33:3781–95. [PubMed: 17089843]

Zhang Y, Chan H-P, Sahiner B, Wu Y-T, Zhou C, Ge J, Wei J, Hadjiiski LM. Application of boundary detection information in breast tomosynthesis reconstruction. Medical Physics. 2007; 34:3603–13. [PubMed: 17926964]

Zhang Y, Pu YF, Hu JR, Liu Y, Chen QL, Zhou JL. Efficient CT Metal Artifact Reduction Based on Fractional-Order Curvature Diffusion. Computational and Mathematical Methods in Medicine. 2011; 2011:173748. [PubMed: 21941593]

Zhao SY, Roberston DD, Wang G, Whiting B, Bae KT. X-ray CT metal artifact reduction using wavelets: An application for imaging total hip prostheses. IEEE Transactions on Medical Imaging. 2000; 19:1238–47. [PubMed: 11212372]

Author Manuscript Author Manuscript Author Manuscript Author Manuscript

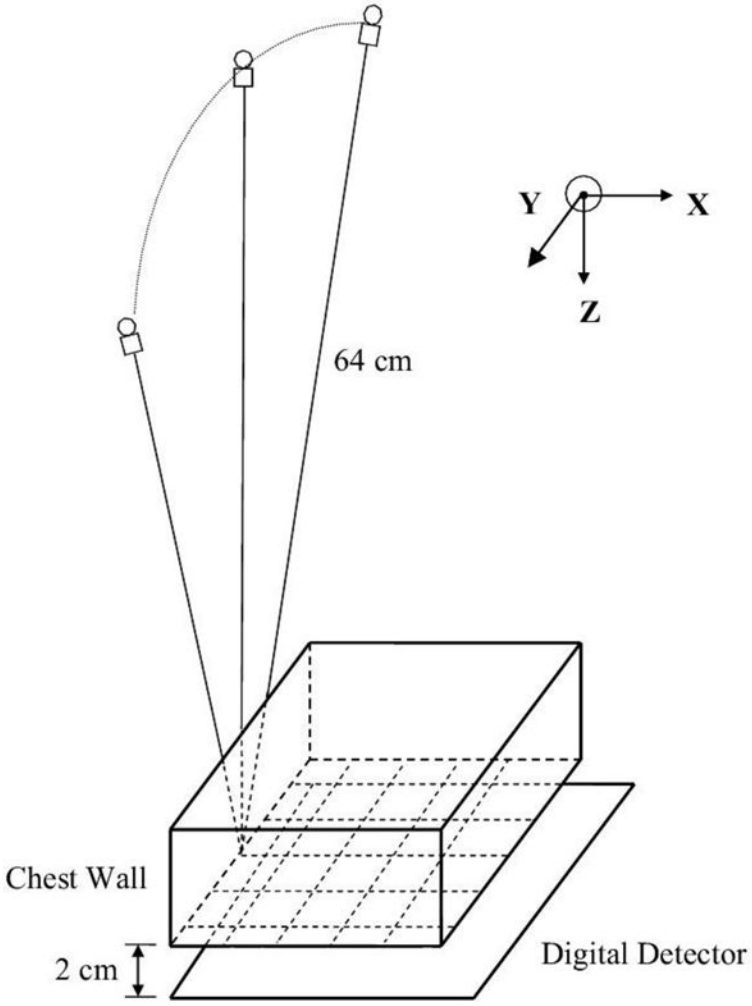

Figure 1.
Geometry of the GE prototype GEN2 digital breast tomosynthesis system used in this study.

Author Manuscript Author Manuscript Author Manuscript Author Manuscript

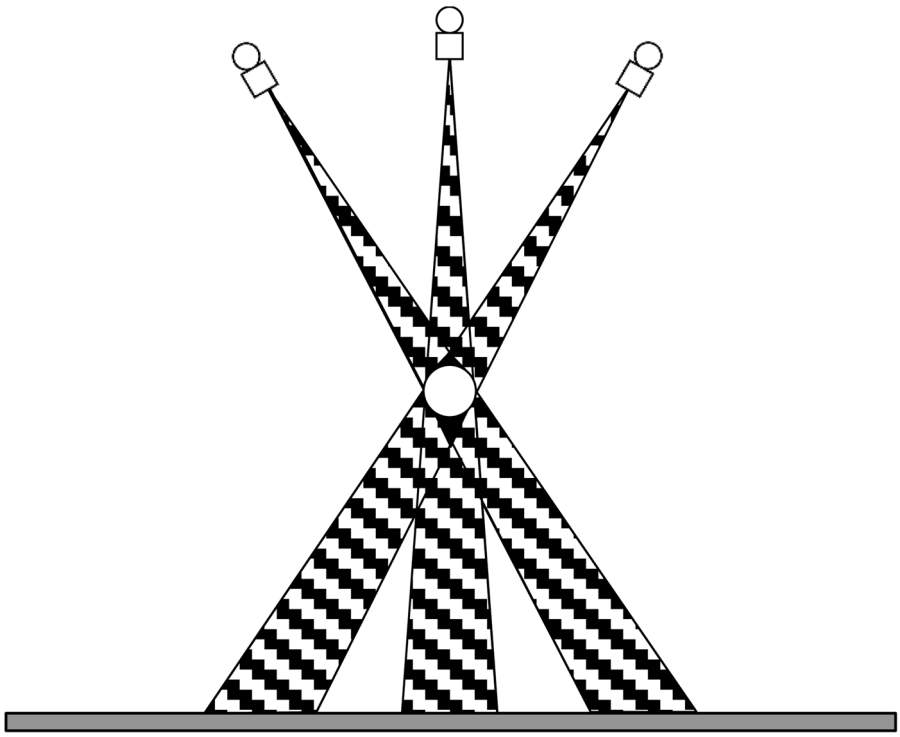

Figure 2.

Projection of a high-attenuation object (white sphere) to the detector from different angles in DBT. Three angles representing the first, central, and the last x-ray source position in a limited-angle tomography geometry are shown. The hatched regions are the conical artifact regions in which the ray paths from each of the source position intersect and are attenuated by the object. The regions where the artifact regions from all angles overlap are shown in black. The voxels in the black regions cannot be updated during reconstruction by any ray that does not intersect the object and therfore the tissue information cannot be recovered. The drawing is not to scale and the distance between the object and the detector plane are exaggerated to demonstrate the effects.

Author Manuscript Author Manuscript Author Manuscript Author Manuscript

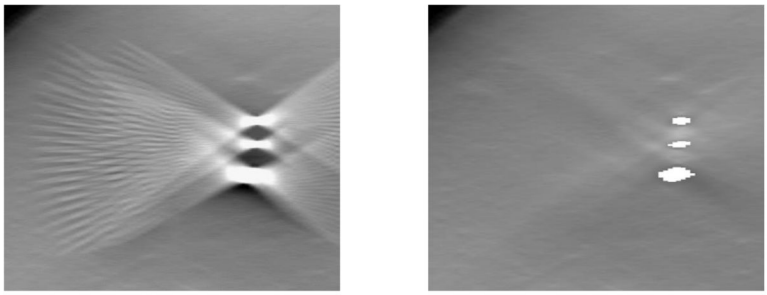

(a) Y-Z plane (Z direction is shown horizontally)

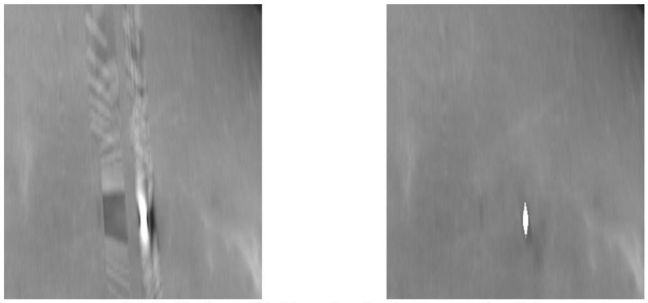

(b) X-Z plane (Z direction is shown vertically)

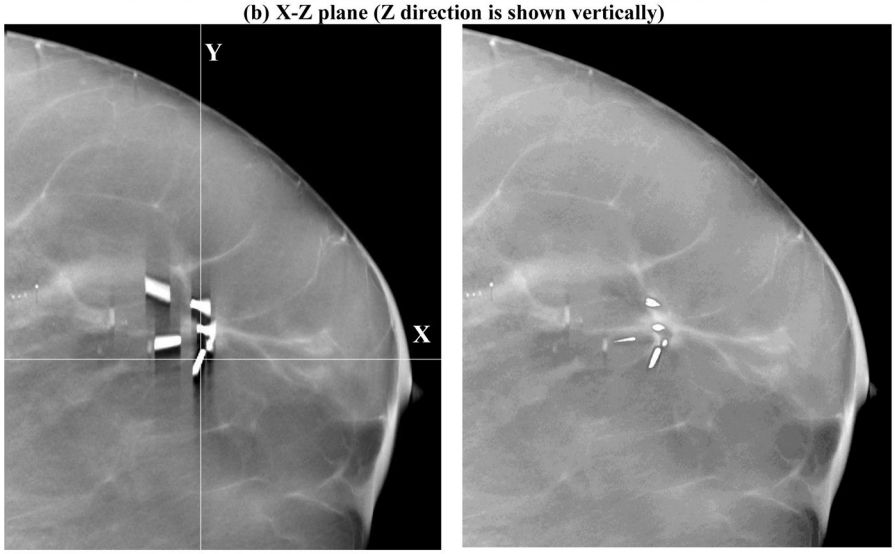

(c) X-Y plane (reconstructed slice)

Author Manuscript Author Manuscript Author Manuscript Author Manuscript

(d) 2D CC-view mammogram

Figure 3.

DBT reconstruction without MAR (left) and with MAR (right) for a breast with multiple lumpectomy metal clips. (a) X–Z plane, (b)Y–Z plane, (c) X–Y plane of the DBT volume. The horizontal line and the vertical line, respectively, in the left image of (c) indicate the location where the X–Z plane and the Y–Z plane intersect the X–Y plane. The voxels where the metal clips are located are refilled with high pixel values to facilitate the radiologist's reading and identifying the previous biopsy site. The shapes of the clips appear irregular because they intersect the DBT slice at different angles. (d) the 2D mammogram of the same breast acquired with a different compression. The breast parenchyma appears more complex than the DBT slice because of the overlap structures. The calcifications in this DBT were not affected by the MAR algorithm; the interplane artifacts from the larger calcifications at different depths can be seen. The visibility of the spiculated tissue region around the metal clips is much better with MAR. The breast was biopsy-proven to have recurring ductal carcinoma in situ and lobular carcinoma in situ.

Author Manuscript Author Manuscript Author Manuscript Author Manuscript

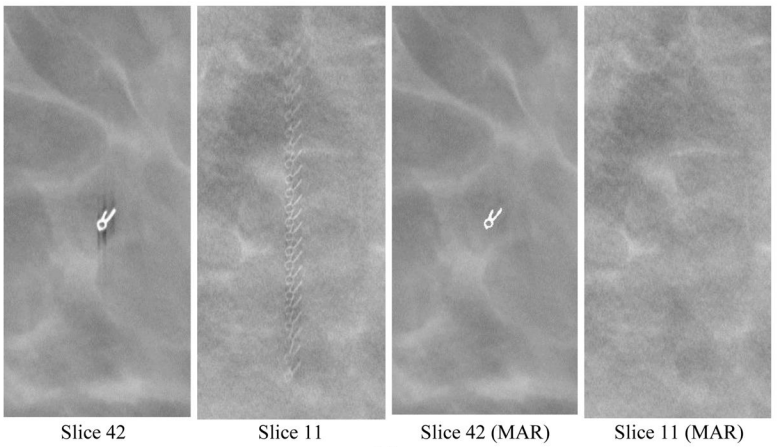

(a)

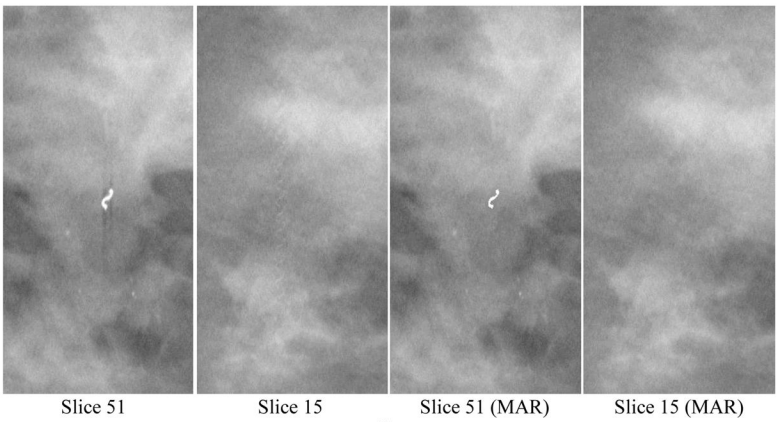

(b)

Author Manuscript Author Manuscript Author Manuscript Author Manuscript

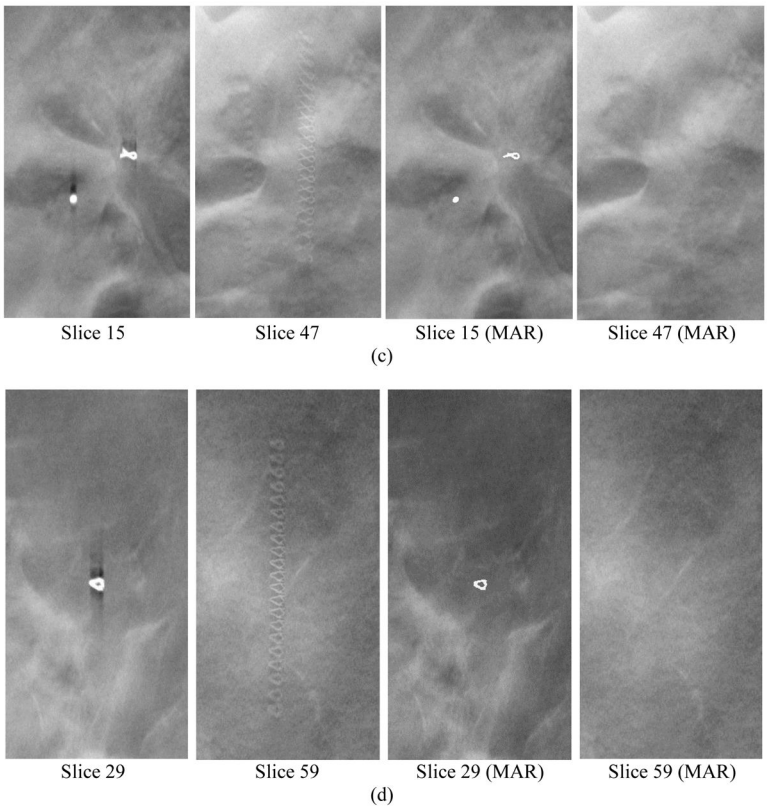

Figure 4.

Examples of core biopsy clips of various shapes in DBT. Each row from left to right: focal plane of clip, interplane artifacts on a slice 3.0 to 3.6 cm from the focal plane, focal plane of clip with MAR, corresponding off-focal plane with MAR. The round object in (c) is a dense benign calcification that also caused artifacts in the reconstructed slices. The calcification was detected and its artifacts were removed in the images with MAR, but it was counted as false positive in this study.

Author Manuscript Author Manuscript Author Manuscript Author Manuscript

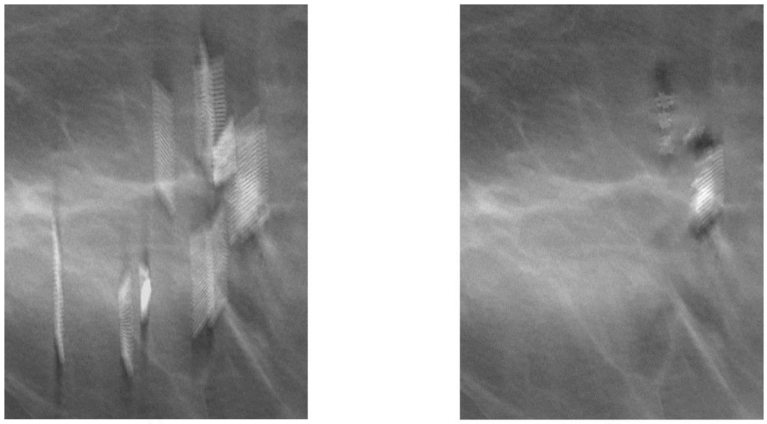

(a) (b)

Figure 5.

A slice in a DBT volume with failed MAR, (a) without and (b) with MAR. Most of the metal clips that did not overlap much were detected and removed. The MAR method failed in some projections for two clusters of clips that were very close together. The artifacts in (b) were partially cleaned up. The removed clips are located at different depths so that the refilled clips are not seen on this slice.

Author Manuscript Author Manuscript Author Manuscript Author Manuscript

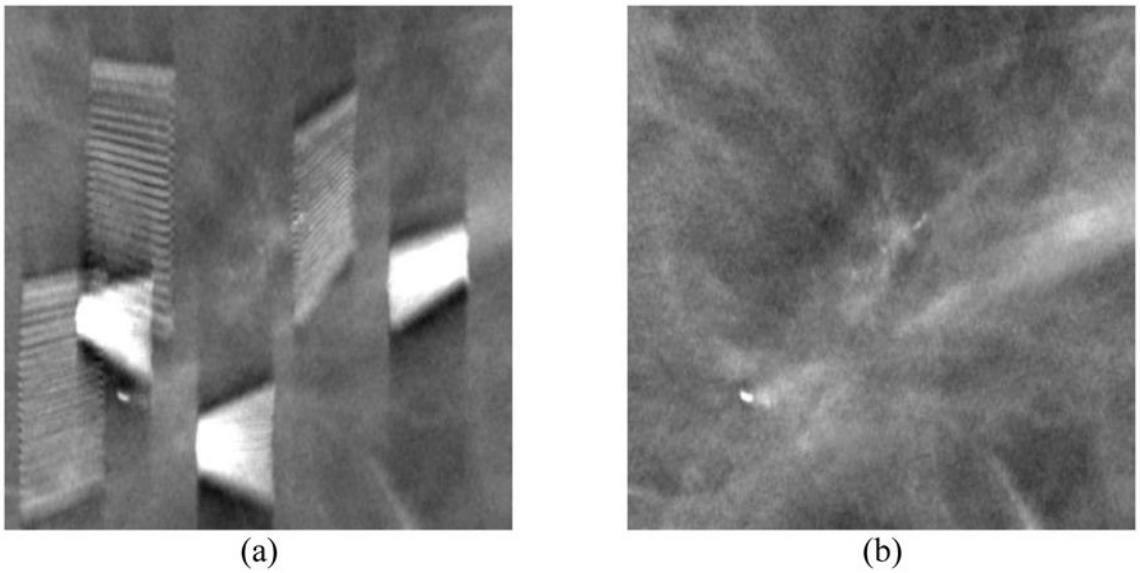

Figure 6.

A DBT slice reconstructed (a) without and (b) with metal artifact correction. The removed clips are located at different depths so that the refilled clips are not seen on this slice. Note the improved visibility of the clustered microcalcifications that were biopsy-proven to be recurring ductal carcinoma in situ

Author Manuscript

Author Manuscript

Author Manuscript

Author Manuscript

Table 1

Performance of metal artifact reduction (MAR) method. A metal marker was successfully removed in the reconstructed DBT view (craniocaudal or mediolateral oblique view) when the metal markers on all projections (PVs) of the DBT scan were detected and replaced by diffusion.

	Training Set	Test Set
Total number of breasts	10	31
Total number of DBT views	19	58
Wide-angle DBT scan	(9 CC, 10 MLO views)	(27 CC, 25 MLO views)
Narrow-angle DBT scan		(3 CC, 3 MLO views)
Number of DBT views with small core biopsy metal microclips	14	36
Number of views with large post-lumpectomy metal markers	9	24
View-based success rate for removal of microclips	100% (14/14)	97.2% (35/36)
View-based success rate for removal of large post-lumpectomy metal markers	100% (9/9)	66.7% (16/24)
False Positives per DBT view	0.05 (1/19)	0.17 (10/58)

Note: A view denotes a breast compression direction in mammography; CC= craniocaudal, MLO = mediolateral oblique.

wide-angle scan: 60° tomographic angle, 21 projections, 3° increments

narrow-angle scan: 16° tomographic angle, 17 projections, 1° increments